FLUCOME 2009
10th International Conference on Fluid Control, Measurements, and Visualization
August 17–21, 2009, Moscow, Russia

VISUALIZATION STUDY OF THERMO-ACOUSTIC INSTABILITIES IN A BACKWARD-FACING STEP STABILIZED LEAN-PREMIXED FLAME IN HIGH TURBULENCE FLOW

V. Sabel'nikov[1], C. Brossard[2], M. Orain[3], F. Grisch[3], M. Barat[2], A. Ristori[2], P. Gicquel[2]

ABSTRACT

Low-frequency combustion instabilities were studied experimentally in a model lean-premixed stepped combustor. The PLIF technique was used to characterize the flame structure. The PIV technique, associated with high-speed visualization of the OH* radical chemiluminescence's emission, allowed to investigate the flow field during the quasi-periodic unsteady flashback when the flame lifted from the edge of the step and moved periodically in and out of the premixing duct. Results strongly suggest that impact of acoustic waves on the flame structure should be taken into account when applying LES approach to industrial gas turbines.

Keywords: Combustion instabilities, turbulent combustion, lean-premixed flame, stepped combustor, PIV, PLIF, high-speed visualization.

INTRODUCTION

Lean-premixed combustion (LPC) has become one of the most promising means of meeting stringent environmental requirements for the reduction of NOx emissions produced by gas turbine engines (Lefebvre, 1995). Operating at lean-premixed conditions, however, often leads to the occurrence of undesirable combustion driven pressure oscillations and intense heat release fluctuations that can severely damage the combustor or turbine hardware. Combustion instabilities occur when pressure oscillations caused by small perturbations in the combustion system grow to the point that they overcome damping forces. If the pressure oscillations are in phase with heat release fluctuations, the Rayleigh criterion is satisfied and the amplitude of the pressure oscillations increases (Rayleigh, 1945). Eventually, pressure oscillations reach a maximal limit when the energy losses become equal to or greater than the energy gains (Culick, 1971). While combustion chamber instabilities can be initialized by numerous different perturbation sources, like flame surface area variations or equivalence ratio fluctuations, it is difficult to determine the exact mechanism responsible for combustion instabilities because they are often system, geometry or operating parameters dependent. The understanding and control of pressure oscillations in the combustor represents one of the most challenging and least understood phenomena potentially

[1] Corresponding author: Office National d'Etudes et de Recherches Aérospatiales (ONERA), Fundamental and Applied Energetics Department e-mail: vladimir.sabelnikov@onera.fr

[2] Office National d'Etudes et de Recherches Aérospatiales (ONERA), Fundamental and Applied Energetics Department

[3] Office National d'Etudes et de Recherches Aérospatiales (ONERA), Physics Instrumentation and Sensing Department

limiting the development of future high performance gas turbine engines.

A substantial amount of careful and valuable results have been obtained so far for LPC instabilities studies, but the majority is not representative of industrial gas turbines conditions. Most of experimental studies were performed on subscale combustors where the global Reynolds numbers (based on the flow parameters in the inlet duct) and turbulent Reynolds numbers are of the order of 10^4 and 10^2, respectively. This corresponds to the regimes of wrinkled and/or corrugated flames in the so-called Borghi diagram (Borghi and Destriau, 1998). Under these combustion regimes, turbulence is not strong enough to significantly impact the flame front internal structure and the statistical characteristics of the combustor instabilities limit cycles. Classically, turbulent combustion models and LES of combustion instabilities are developed mainly for these two regimes. However, typical flames in industrial gas turbines are characterized by much higher turbulent Reynolds numbers ($\mathrm{Re}_t \geq 10^3$). As a consequence, combustion takes place in thickened highly disconnected flame pockets (thickened wrinkled flames regime in the Borghi diagram), and the limit cycle of combustion instabilities is significantly influenced by turbulence.

The present study focuses on highly turbulent lean-premixed methane/air flames. In this paper, the experimental setup, optical diagnostics techniques and first results are presented. A more comprehensive analysis of the results will be made available in a next publication. Experiments were carried out on the ONERA/LAERTE model stepped combustor of rectangular cross section with a sudden expansion at the combustor inlet (backward-facing step) and downstream contraction at the combustor outlet. This backward-facing step configuration was studied extensively during the last fifty years (e.g., Ganji and Sawyer, 1980, Pitz and Dailly, 1983, Cohen *et al* 2003). Despite some simplifications in the geometry of the combustor, it allows to reproduce the most important elements of the gas flow in real combustors, such as recirculation zones and shear layers. The main objective of this study is to provide further insight into the mechanisms of combustion instability leading to quasi-periodic unsteady flashback when the flame lifts from the edge of the step and moves periodically in and out of the premixing duct. Both stable and unstable modes of combustor operations were investigated. Qualitative planar laser induced fluorescence (PLIF) of the OH radical, as well as high speed intensified video camera visualizations (4,000 frames/s) of the OH* radical chemiluminescence emission were used to detect flame structure and interactions between the flame front and large scale vortex. Instantaneous velocity fields were obtained using particle image velocimetry (PIV) and synchronized with the recording of high-speed movies.

EXPERIMENTAL SETUP

Stepped Combustor

A schematic view of the ONERA/LAERTE stepped combustor is presented in Fig. 1.

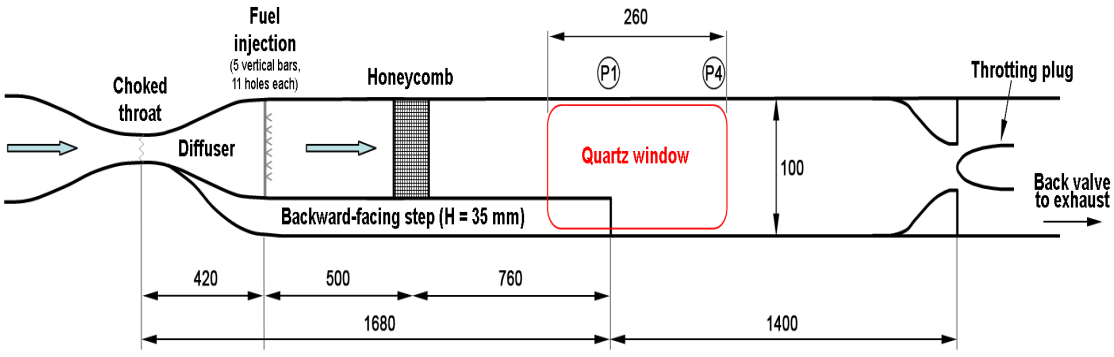

Fig. 1. Schematic view of the ONERA/LAERTE stepped combustor

The water-cooled combustion facility consists of a 1.7-m long inlet duct, a 1.4-m long dump (backward-facing step) combustor, and an exhaust nozzle. The facility is supplied with preheated air with a maximum temperature of 650 K. Air maximum flow rate is 600 g/s. Preheated air is delivered to the facility through a choked nozzle located at 1.7 m upstream from the combustor inlet. Then the preheated air passes through the inlet (premixing) duct before entering the combustor. The inlet duct is comprised of several rectangular-section (100×65 mm²) pipes. The methane injector, made of five vertical bars pierced with a total of 55 holes, was placed 1.26 m upstream from the step. Downstream of the injector was a honeycomb grid, which straightened the flow, reduced the turbulence level and improved the homogeneity of the airflow. The thickness of the boundary layer (measured by a Pitot tube) at the step section was about 13 mm. Velocity profile corresponded to a fully-developed turbulent boundary layer and was well-described by a 1/7 power law. The fuel and air lines were metered by sonic nozzles. The step is 35-mm high, and the 1.4-m long chamber has a square section of 100×100 mm². The test section is equipped with 100-mm high by 260-mm long UV-glass windows on 3 sides (upper and both lateral) of the combustor to provide optical access to the flame. A spark igniter is inserted through the lower combustor wall. It is mounted flush with the surface. The exit nozzle has an adjustable plug that is used to modify the chamber pressure and acoustic impedance. The tests were performed over a range of air inlet velocity $U_0 = 40 - 65$ m/s, inlet air temperature $T_{air} = 450 - 600$ K, fuel-air equivalence ratio ER = 0.8 – 1.0, air mass flow rate $m_{air} = 200 - 350$ g/s, Reynolds number based on the flow parameters in the inlet duct $Re_H = 10^5 - 3.10^5$, turbulent Reynolds number $Re_t = 10^3 - 2.10^3$, chamber pressure P = 1.12 - 1.5 bar and thermal power of the chamber 550 – 830 kW. Acoustic pressure measurements were performed at two axial locations in the combustor tunnel, indicated in Fig. 1: P1 and P4 – at 1.5 cm and 67.5 cm downstream of the step, respectively. Pressure oscillations were detected by ¼ in. (6.3 mm) Bruel&Kjaer microphones (type 4136 and 4938) mounted on waveguides and equipped with preamplifiers. The microphones are positioned at 80 cm from the ports located on the upper wall (opposite the step) of the model by using a connecting duct. This duct is terminated by a 10 m-long coil pipe, which eliminates reflected waves.

Optical Setup for PLIF Technique

Only a short description of planar laser induced fluorescence (PLIF) of the OH radical (OH PLIF) is given here. A schematic view of the optical setup is displayed in Fig. 2. A single, 6 ns, 20 mJ pulse from a frequency-doubled, Nd:YAG-pumped dye laser (Quantel YG780) was formed into a collimated sheet using one spherical and two cylindrical lenses. The first two lenses, -50 mm and 300 mm focal lengths, formed a cylindrical telescope which spread the laser beam into a collimated, 50-mm wide sheet. The spherical lens, 1 m focal length, focused the sheet to a 150 μm waist. The laser was tuned to the $Q_1(5)$ transition of the (1,0) vibration band of the ($X^2\Pi$-$A^2\Sigma^+$) system of OH at 282.75 nm. This transition was chosen due to its strong intensity and its weak dependence with temperature: as a consequence, the recorded fluorescence intensity is directly proportional to the concentration of OH radicals. The laser linewidth was measured to be approximately 0.1 cm^{-1} by recording the spectral profile of several OH transitions in a premixed methane-air reference flame. The laser was tuned to the line-centre of the OH transition using the reference flame. Fluorescence signal was recorded using an intensified CCD camera (Princeton Instruments, Imax) with an intensifier gate width of 200 ns. The CCD array was 512 by 512 pixels and the frame rate of the system was 3 Hz. The ICCD camera was equipped with Schott spectral filters WG295 and UG5 and a 94 mm, f/4.1 UV lens. The vertical laser sheet was first placed along the flow axis and at various axial locations downstream of and upstream from the step. A 50 × 100 mm area of the flow field was imaged onto the camera, so that the spatial resolution was 195 μm per pixel. The vertical laser sheet was then placed in the transverse direction in order to investigate the flame structure in a cross-section of the flow, at two longitudinal locations: 20 mm upstream from and 40 mm downstream of the step.

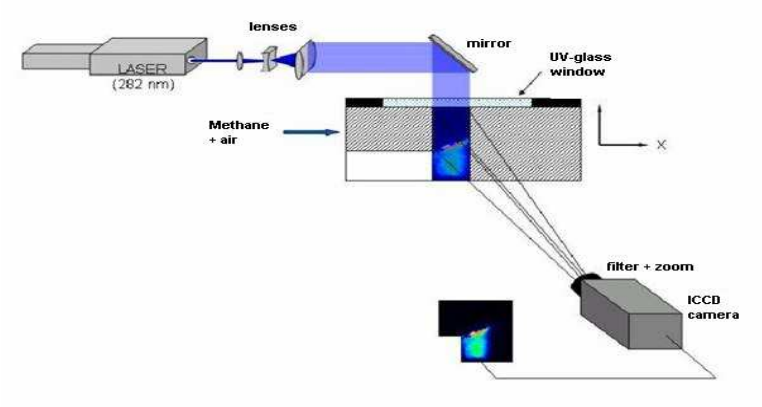

Fig. 2. Schematic view of the experimental setup for PLIF technique

Conversion of fluorescence signal into concentration of OH radical requires taking account of different parameters, which influence the quality of measurements. Raw images must be corrected for camera dark background, flat field non-uniform response of the camera, collection optics, temporal fluctuations and spatial distribution of laser energy. An instantaneous correction must be systematically performed in order to eliminate this bias. The flat field corrections were made using static cell in-situ measurements of acetone fluorescence. The laser sheet energy and its spatial distribution were measured using a cell filled with acetone vapor as a reference channel.

Because LIF signals are temperature-dependent, the absolute number density of OH has to be calibrated beforehand in a flame where OH concentration, temperature and pressure are well known. The calibration was performed in a laminar premixed methane/air flame with an equivalence ratio of 0.9, recording OH fluorescence intensity versus height above the porous surface. Measurements were carried out with experimental conditions (optical beam path, pulse energy, distance between the laser and the probe volume, ICCD gain,…) similar to those encountered with the stepped-combustor. Absolute concentration was obtained from comparison between experimental and theoretical profiles for the same flame conditions. The flame was modeled as one-dimensional using the CHEMKIN and PREMIX computer codes (Kee *et al* 1989). The resultant comparison gives the calibration law, i.e. the number of photons emitted by OH radicals versus their absolute concentration [molecules/cm^3]. Quenching rate effects from H2O were minimized in the calibration procedure by choosing a flame condition for which the H2O concentration is similar to that found in the combustor.

Optical Setup for PIV Technique Synchronized with High-Speed Visualizations

The Particle Image Velocimetry (PIV) technique is used to measure the instantaneous velocity field in a planar cross section of the observed flow. Because the principle is well-known (see for instance Raffel *et al*, 1998), only a short description of the technique is given here. The investigated flow is seeded with small-sized particles (solid particles or liquid droplets depending upon the nature of the fluid and the temperature range in the flow). The fluid velocity is determined by measuring the displacement of the particles over a given time duration. Two laser sheets separated by an adequate time interval are pulsed consecutively to illuminate the tracer particles through the image zone. The light scattered by the particles located into the laser sheet is collected onto a CCD camera where each exposure is recorded in a separate frame. The images are divided into small interrogation windows, the size of which determines the spatial resolution of the measurement. The displacement of illuminated particles inside each interrogation window is then determined by computing a spatial cross-correlation function between the two consecutive images. The velocity vector projected onto the laser sheet is then deduced.

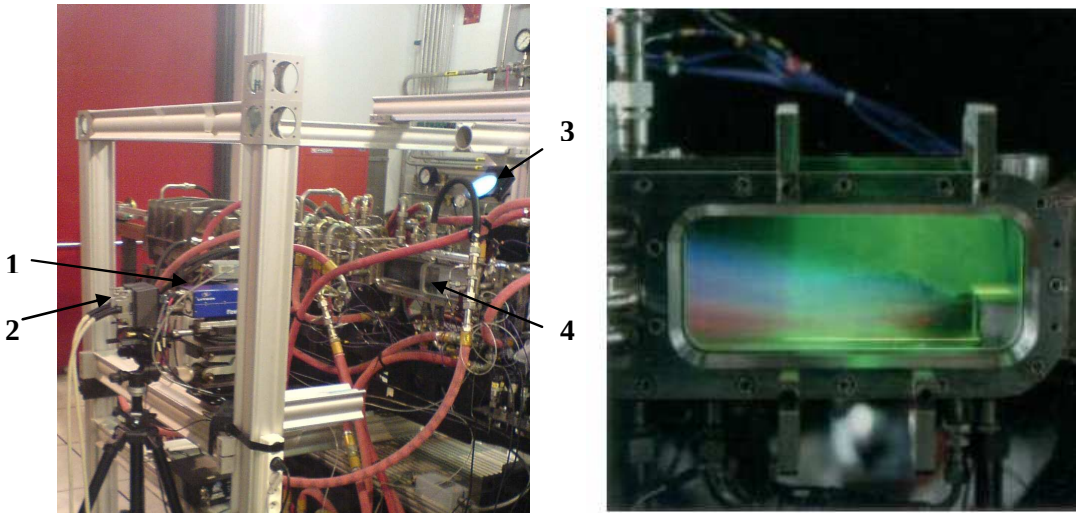

Fig. 3. Photos: a) PIV and high-speed intensified video camera setup around combustor, 1: PIV camera; 2: high-speed camera; 3: 100 mm diameter mirror for laser sheet; 4: combustion chamber; b) combustion chamber with flame anchored at the step, illuminated with vertical PIV laser sheet

Fig. 3a shows a photo of the PIV setup and high-speed intensified video camera around the stepped combustor. Two superimposed diverging laser sheets at 532 nm wavelength were formed from a double oscillator, frequency-doubled pulsed Nd:YAG laser system (Quantel Twins CFR, 120 mJ/pulse). The laser sheets were placed vertically along the flow axis by using a 100 mm diameter mirror located above the upper window, as shown in Fig. 3a. Fig 3b shows a photo of the combustion chamber with the flame anchored at the step, illuminated with vertical PIV laser sheet (regions upstream from and downstream of the step are seen). The time interval between the two consecutive laser pulses was set to 3 µs for the experiments reported in this paper. The flow was seeded upstream of the methane injector with solid tracer particles using a pressurized cyclone generator. Magnesium oxide particles, capable of withstanding the high-temperature reacting environment, were chosen. The size distribution of the particles is centered on 1 µm. These particles were slightly diluted with nanometric Aerosil® (fumed silicon dioxide) particles in order to fluidize the seeding particles mixture and reduce the risk for particles agglomeration. Particles images were collected perpendicularly to the laser sheets, through one of the chamber lateral UV-glass windows, as shown in Fig. 3a, using a CCD camera (LaVision® Flowmaster 3S), with a frame size of 1280x1024 pixels. The camera was equipped with a 50 mm, f/8 lens and a narrow-band interference filter centered at 532 nm wavelength (3 nm FWHM bandwidth) in order to filter out the flame radiation. The field-of-view covered the whole height of the chamber (100 mm) and a 130 mm length (65 mm on either side of the step). Image acquisition and data reduction were performed using the Davis 7.1 software from LaVision®. In order to reduce the background noise generated by window pollution from MgO particles deposits, particularly significant in the recirculation zone located downstream of the step, images were systematically pre-processed using a subtract-sliding-background type numerical filter. Cross-correlation interrogation windows of 32x32 pixels with 50% overlap were used, corresponding to a measurement spatial resolution of 3.25 mm and a vector every 1.6 mm.

The high-speed intensified video camera (Photron Fastcam-ultima APX-i2) was placed near the PIV camera, as shown in Fig. 3a, and viewed the chamber with a slight tilt angle. It was equipped with a

narrow-band filter (CVI Technical Optics Ltd) centered at 310 nm wavelength (10 nm FWHM bandwidth) in order to select a spectral region in which the only flame radiation source is OH* chemiluminescence emission. The frame rate of the camera was 4,000 frames/s, for a frame size of 1024x512 pixels. For each image, the intensifier was operated during the last 150 µs of the 250-µs CCD array exposure. This time duration was found to be the best compromise between sufficient signal-to-noise ratio and low exposure time. Signals from microphones located at P1 and P4 (see Fig. 1) were recorded simultaneously to the images at a 40 kHz data rate by using a multi-channel data link system associated with the camera. The PIV images and high-speed images acquisitions were synchronized following the scheme represented in Fig. 4. The synchronization allowed a timing identification of the instantaneous PIV velocity fields with respect to the flame movement. The PIV acquisition unit and the high-speed cameras were the master and slave systems, respectively. At each trigger signal from the PIV system, a 30-ms sequence of 121 chemiluminescence images was recorded. The two PIV images were recorded in the middle of the sequence. A total of 101 such sequences were successively recorded at a 2.5 Hz acquisition rate, after which the memory of the high-speed camera was filled.

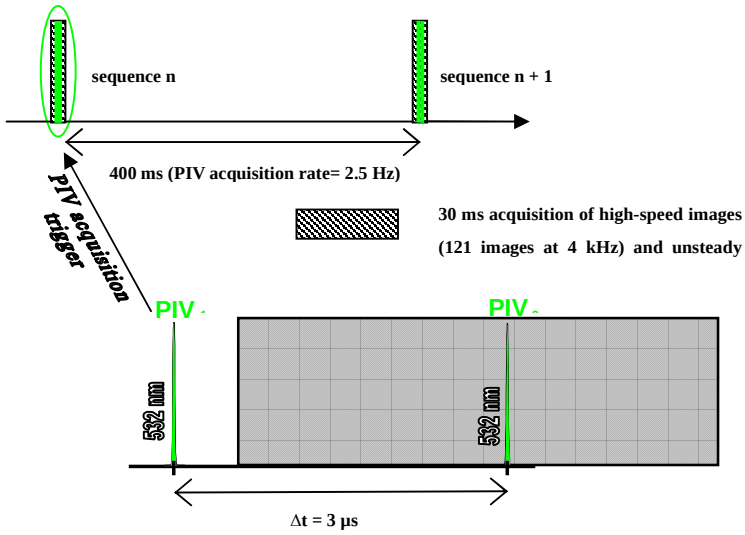

Fig. 4. PIV/high-speed camera synchronization scheme

It should be reminded here that, on one hand, contrarily to PLIF, which is a planar technique, emission images are integrated over the chamber width (line-of-sight technique). Moreover, due to the large exposure time, the time resolution of the emission images is quite poor (150 µs exposure time, versus 6 ns pulse duration for PLIF), and the observed flame image can not be "frozen" due to significant fluid motion during the exposure. On the other hand, because the OH* radical, on an electronic excited state, exists only in the flame front, the chemiluminescence signal is a much more reliable tracer of the reacting zone than the fluorescing OH, which is in the fundamental electronic state and exists not only in the flame front, but also in the burnt gas. Moreover, the acquisition rate of the PLIF technique is limited to a few Hz (3 Hz in this study, versus 4,000 Hz for high-speed chemiluminescence images) and does not provide access to unsteady information. Therefore, the high-speed chemiluminescence visualization and PLIF techniques complement each other: the PLIF technique provides excellent time and space resolution; the high-speed visualization provides detailed qualitative characterization of the flame unsteadiness.

EXPERIMENTAL RESULTS

Classic stable turbulent combustion was observed when the exit nozzle was fully open, under the following conditions: $P = 1.12$bar, $\phi \geq 0.8$, $T_{air} \geq 500$ K and $U_0 \geq 40$ m/s. High-speed visualization,

instantaneous OH PLIF images and pressure power spectra (not presented here) show that stable turbulent combustion is characterized by a strong influence of irregular turbulent vortex movements on the coherent vortex structures generated in the mixing layer downstream of the step. Power spectra do not exhibit any pronounced peaks, and it can be concluded that stable turbulent combustion consists actually of numerous coexisting instabilities. High-speed visualization and PLIF images reveal that there is some permanent flame flapping with finite amplitude. The images show that the flame is primarily anchored at the initial part of the shear layer generated by the backward-facing step. The flame stabilization location fluctuates with small amplitude at the vicinity of the step edge during this flapping.

Increasing the degree of constriction of the combustor exit nozzle (that, in turn, increased the mean combustor pressure and changed the acoustic impedance) performed transition from stable to unstable combustion. The instability appeared at pressures larger than 1.25 bar. To improve the understanding of the mechanisms involved, one case was studied in detail: U_0 = 51m/s, ϕ = 0.82, T_{air} = 550 K, air mass flow 270 g/s, combustor pressure 1.35 bar. Power spectrum of the pressure signals has a 154 dB peak at the low frequency of 66 Hz (it corresponds to the ¼ longitudinal acoustic wave for the inlet duct). However, the pressure signals were highly modulated in frequency (in the range 55-80 Hz) and amplitude, and exhibited abrupt low-frequency drops toward zero (around 2 Hz), as shown in Fig. 5. This modulation behavior prevents from locking images acquisition (PIV, PLIF or chemiluminescence) to the phase of the unsteady pressure signal, a method frequently used in combustion instabilities studies for moderate Reynolds numbers (see for instance Broda *et al* 1998, Lee *et al* 2000, Docquier and Candel, 2002, Lee and Santavicca, 2003, Ghoniem *et al* 2005)) in order to fully resolve a cycle of instability.

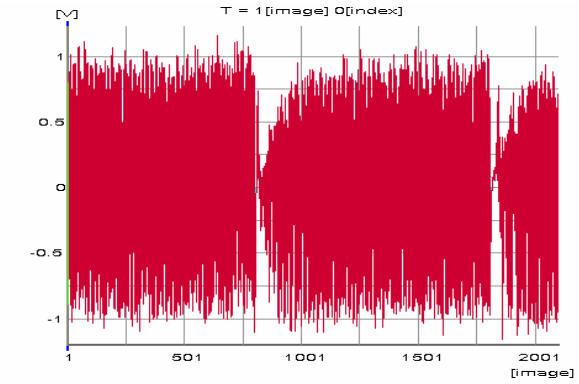

Fig. 5. Sample of an unsteady pressure signal recording, showing in particular low-frequency (around 2 Hz) pressure drops toward zero

A trigger threshold that defines the time origin can not be applied due to the modulation in amplitude, and the modulation in phase prohibits triggering laser flash lamps that require constant frequency operation. However, the simultaneous recording of high-speed chemiluminescence images and pressure signals allowed to link directly the evolution of the reaction zone with that of the unsteady acoustic pressure, as represented in Fig. 6 in which sampled images are gathered with corresponding pressure traces P1. The flame is first anchored at the step edge. As the pressure decreases from maximum to minimum, the flame propagates up to sometimes more than 65 mm (i.e. around twice the step height) upstream from the step. The window is not large enough to visualize the flame front more upstream. Then the flame propagates back downstream toward the step as the pressure increases. Finally the flame gets re-anchored at the step edge, and the cycle repeats itself. The flame location in the last image in Fig. 6 is close to what can be observed for the case of a stable flame. The flame propagation upstream takes around 8 ms, while the flame returns toward the step much faster, during only around 2 ms. This timing difference can be explained by opposite directions of the flame velocity and acoustic velocity while the

flame propagates upstream, versus same directions when it propagates downstream. It also explains the non-sinusoidal shape of the pressure signal: the pressure decreases or increases with different and high slopes during flame propagation upstream and downstream, and decreases very slowly from the start of the flame re-attachment process to the flame detachment.

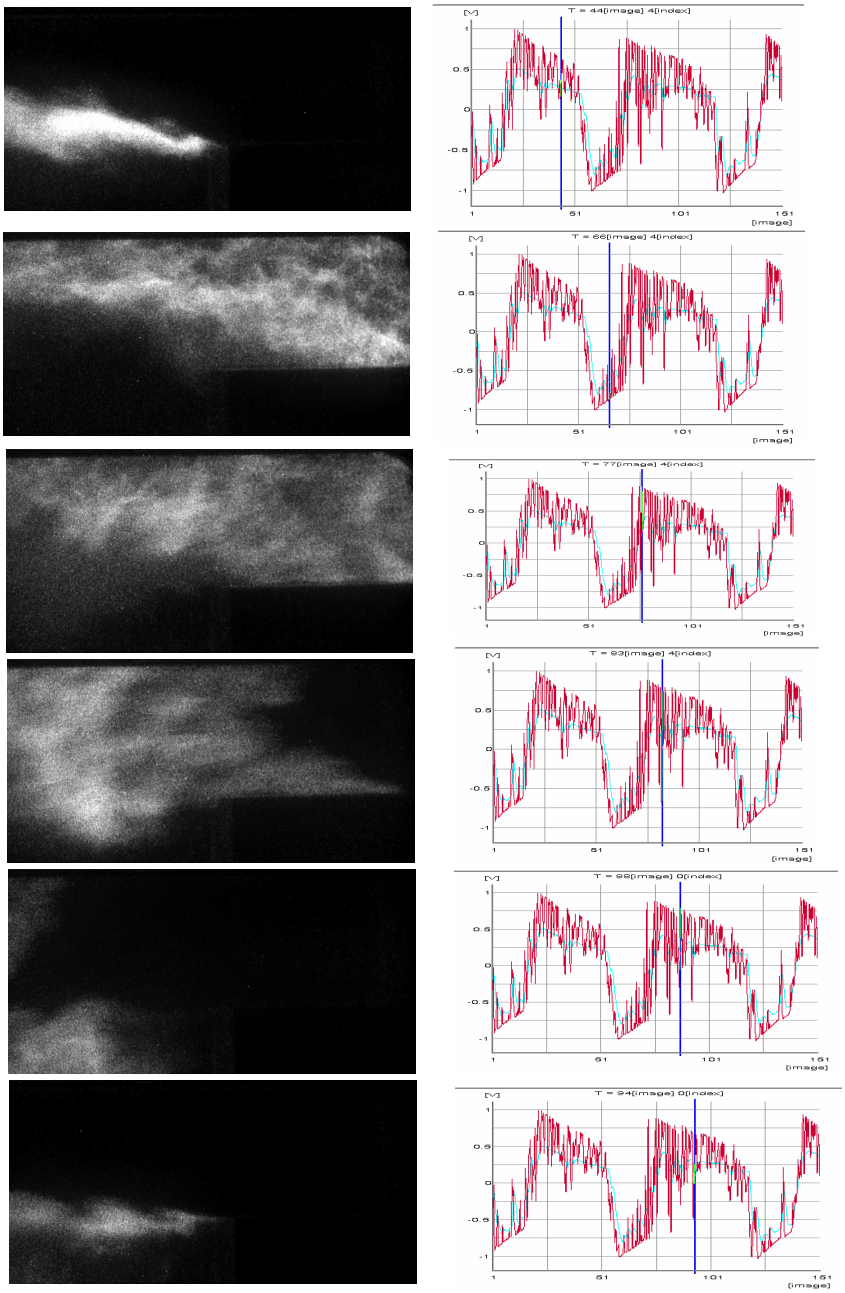

Fig. 6. Simultaneous recording of high-speed OH* chemiluminescence images and unsteady pressure P1 (blue: low-pass filtered, red: unfiltered) during a cycle of instability

Fig. 7 shows an example of an instantaneous PIV velocity field synchronized with high-speed images taken as the flame propagates downstream toward the step before re-attachment. This result shows that this motion is associated with the formation of a strong vortex behind the step and an induced acceleration near the step edge, with a velocity in this region reaching 85 m/s versus 40 m/s upstream from the step at this instant in the cycle. Fig. 7 illustrates the interest of synchronizing PIV acquisition with high-speed chemiluminescence images: although the pressure signals do not allow phase-locked acquisition, the synchronization allows identifying at which instant, pressure, and flame location of the cycle, the velocity field corresponds to. The procedure can be repeated for all recorded instantaneous velocity fields in order to fully describe the fluid motion during a cycle of instability. However, this post-processing task is quite time-consuming and has not been completed yet.

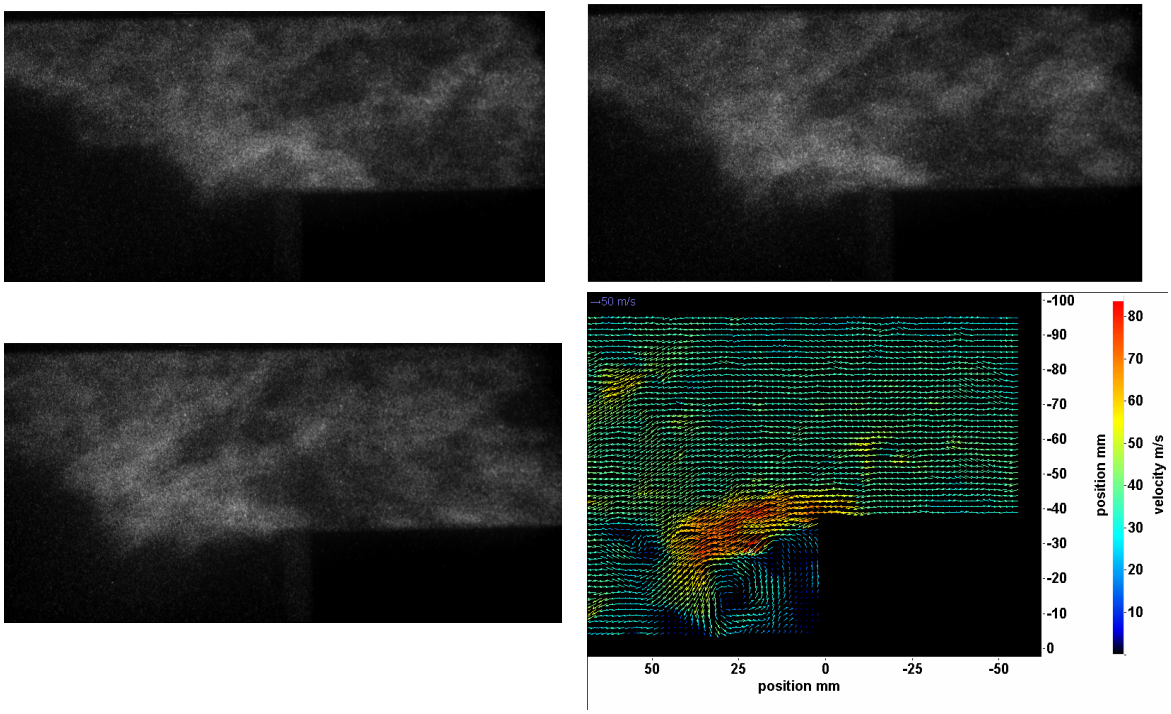

Fig. 7. Instantaneous PIV velocity field synchronized with high-speed OH* chemiluminescence images at 4,000 Hz.

Figs 8 and 9a show the average and fluctuating velocity fields, deduced from 101 instantaneous samples for a stable flame, respectively. The large recirculation zone behind the vortex is clearly evidenced from the average velocity field. The longitudinal component of the velocity upstream from the step is 70 m/s, with an rms fluctuation of around 10 m/s. As expected, the largest fluctuations occur in the reacting mixing layer, with a fluctuation level less than 20 m/s. The difference between stable and unstable cases is particularly strong when comparing in Figs. 9a and 9b the fluctuation level of the velocity longitudinal component upstream from the step. These fluctuations reach 45 m/s rms for the case of an unstable flame, due to the periodic unsteady flashback observed on the high-speed movies, when the flame lifts from the edge of the step and moves periodically in and out of the premixing duct. Some of the instantaneous velocity fields revealed some particularly high levels of velocity when the flame moves toward the step from the premixing duct, such as in Fig. 10a showing velocities reaching 200 m/s. On the contrary, some cases of flow reversal were observed, such as in Fig. 10b showing negative velocities of up to 40 m/s in level near the step wall.

PLIF images provided further insight into the flame structure during instabilities thanks to its excellent time and space resolution characteristics. A cycle of instabilities was reconstructed in Fig. 11a from selected instantaneous images, taken when the left border of the 50x50 mm laser sheet, placed along the flow axis, was located 10 mm upstream from the step. Instabilities are mainly observed as large-amplitude and extremely strong flapping of the flame. These violent oscillations are driven by periodic vortex shedding from the step edge. The flame stabilization location is moved by large–scale vortices on a large zone of the combustor. Consequently, the vortex shedding is controlled by large acoustic velocity fluctuations at the step edge where the flow separates, which provides the coupling between combustion, vortices and acoustics. From PLIF images, the features of the turbulent combustion regime can also clearly be visualized, through the presence of small wrinkled structures.

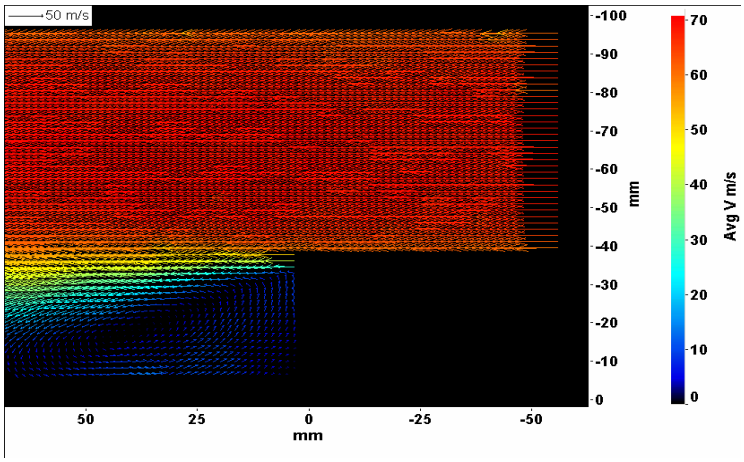

Fig. 8. Average velocity field obtained from 101 instantaneous PIV velocity fields for a stable flame. False-colors refer to the module of the velocity vector. The step edge is located at x = 0, y = -35 mm

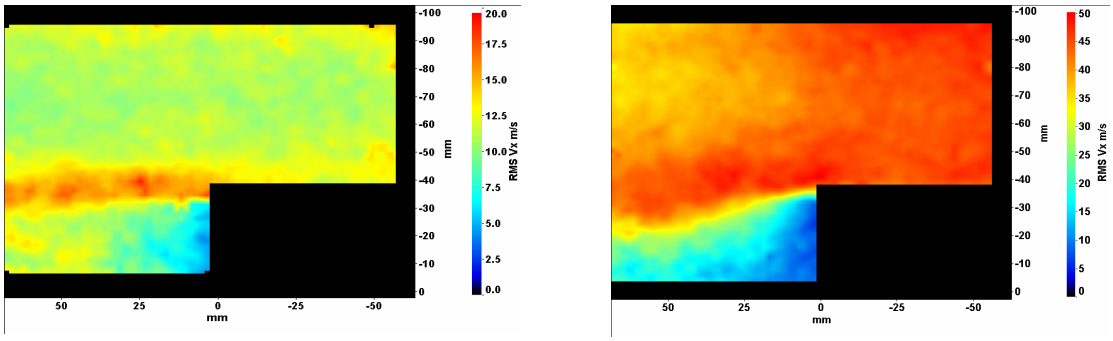

a) **b)**

Fig. 9. RMS scalar field of the longitudinal velocity component obtained from 101 instantaneous PIV velocity fields, a) stable flame, b) unstable flame

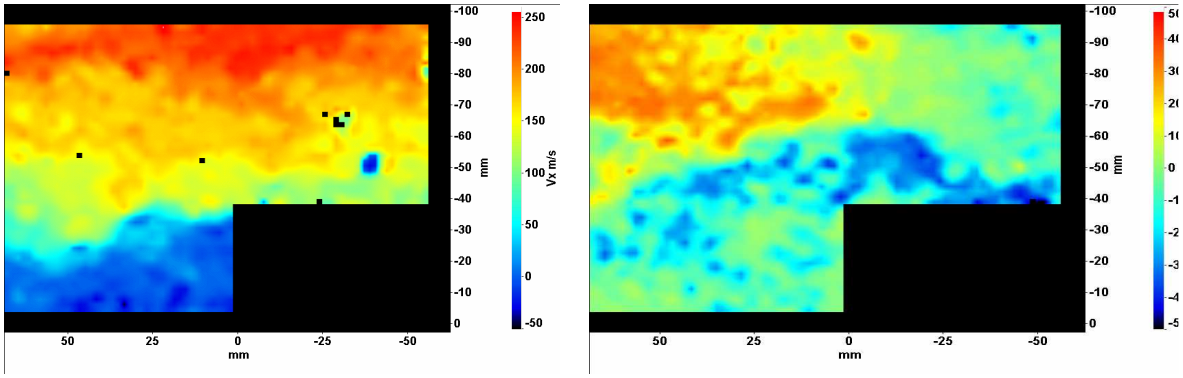

a) b)

Fig. 10. Instantaneous velocity fields showing very high velocity fluctuations occurring during instabilities. Black squares correspond to interrogation windows in which no valid vector could be measured, a) very high velocities, up to 200 m/s (red zones), b) flow reversal (negative velocities in the blue zones)

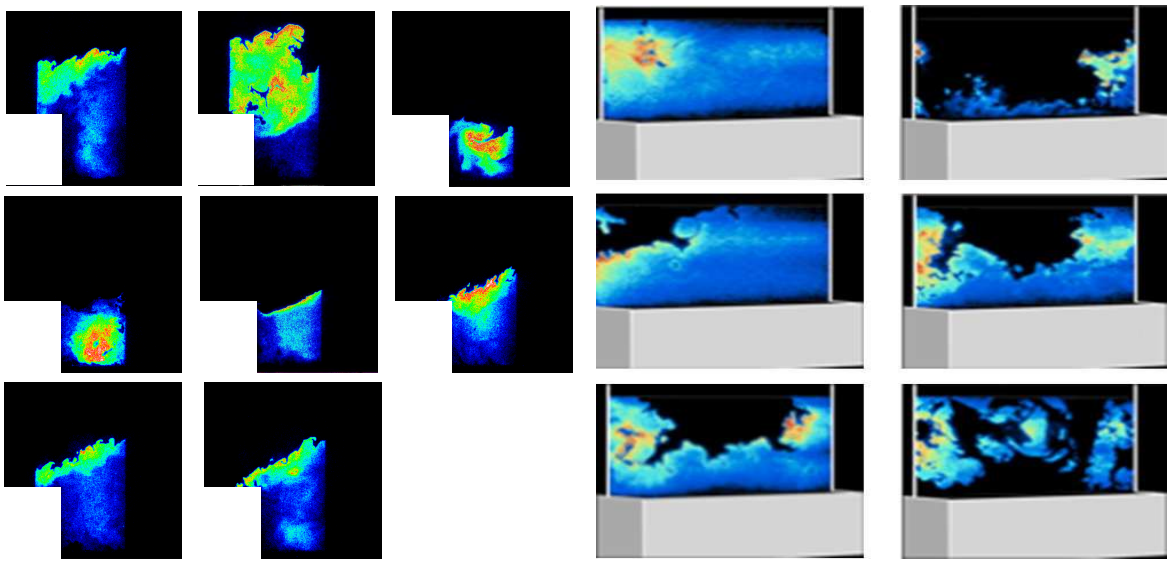

a) b)

Fig. 11. Typical instantaneous PLIF images taken during unstable combustion, a) reconstructed cycle of instability from sample images taken with laser sheet along flow axis, b) sample images taken with laser sheet perpendicular to flow axis, at -20 mm upstream from the step.

Such structures, sometimes as small as a few hundred microns, are particularly noticeable in Fig. 11b, representing PLIF images recorded when the laser sheet was placed perpendicularly to the main flow, at about 20 mm upstream from the step. Also visible are some methane/air combustion pockets disconnected from the main flame, typical for the thickened wrinkled flames regime in the Borghi diagram. A striking feature revealed by PLIF images taken in the transverse direction is that the flame is highly three-dimensional and largely distributed over volume, especially when unstable. In the unstable case, the flame spatial location varied with time: it could either spread over the entire cross-section, or be located near the sidewalls (glass windows) with partial extinction along the flow axis. Such a variation of the flame spatial location was not observed for the stable case; downstream of the step, the flame remained quite uniformly spread over the chamber width, and never occupied the entire height of the chamber. These results suggest the strong influence of wall conditions on the spatial development of the flame.

The phase and frequency modulation of the pressure oscillations reported in this study may be attributed to these particular features of the turbulent combustion regime identified by PLIF images. As indicated in the introduction section of this paper, most of experimental studies were performed on subscale combustors with lower turbulent Reynolds numbers and therefore different turbulent combustion regimes (wrinkled or corrugated flames), classically assumed in LES of combustion instabilities; in these studies, the phase and frequency modulation observed here is not reported. In our experiments, strong turbulence most likely significantly impacted the flame front internal structure and the statistical characteristics of the combustor instabilities limit cycles. This is an important result since the thickened wrinkled flames regime at play is typical for real combustors in industrial gas turbines. Therefore, the obtained results suggest that some modifications of turbulent combustion modeling are needed when applying LES approach to industrial gas turbines; in particular, impact of acoustic waves on the flame structure has to be taken into account.

CONCLUSION

In this paper, recent progress in the study of combustion instabilities inside a lean-premixed stepped combustor has been described. Transition from stable to unstable regime of combustion occurred when the pressure was increased above 1.25 bar. High-speed OH* chemiluminescence images, synchronized with PIV measurements and pressure signals, allowed to describe the fluid motion and to link directly the evolution of the reaction zone with that of the unsteady acoustic pressure during quasi-periodic cycles of unsteady flashbacks, when the flame lifted from the edge of the step and moved periodically in and out of the premixing duct. Flame propagation up to more than twice the step height upstream from the step was observed during flashback. These quasi-periodic flashbacks are associated with very large velocity fluctuations; at times, velocity levels of up to 200 m/s were measured upstream from the step, to be compared with an average velocity of 70 m/s in the stable case. On the contrary, some periods of flow reversal, i.e. negative velocities upstream from the step, were detected. Power spectrum of the pressure signals showed a dominant 154 dB peak at the low frequency of 66 Hz, but with significant modulation in amplitude and frequency. This modulation is attributed to the features of the turbulent combustion regime, identified by PLIF images. The flame is composed of very small wrinkled structures, sometimes as small as a few hundred microns, as well as of disconnected methane/air combustion pockets. The flame is also highly three-dimensional and largely distributed over volume, and exhibits significant time variation of spatial location when unstable. In the experiments reported in this paper, strong turbulence most likely significantly impacted the flame front internal structure and the statistical characteristics of the combustor instabilities limit cycles. This is an important result since the thickened wrinkled flames regime at play is typical for real combustors in industrial gas turbines. Therefore, the obtained results suggest that some modifications of turbulent combustion modeling are needed when applying LES approach to industrial gas turbines; in particular, impact of acoustic waves on the flame structure has to be taken into account.

ACKNOWLEDGEMENTS

The authors would like to acknowledge the Direction Générale de l'Armement (French ministry) for partly funding this study.

Special thanks are also expressed to Michel Poirot, Patrick Roux, Bruno Rouxel and David Carru for their technical support.

REFERENCES

Borghi, R., Destriau, M. (1998), La combustion et les flammes, Editions Technip, Paris, France.

Broda, J.C., Seo, S., Santoro, R.J., Shirhattikar, G., Yang, V. (1998), "An experimental study of combustion dynamics of a premixed swirl injector", 27th Int. Symp. On Combustion, 1849-1856.

Cohen, J.M., Wake, B.E., Choi, D. (2003), "Investigation of Instabilities in a Lean Premixed Step Combustor", J. Propulsion and Power, **19**(1), 81-88.

Culick, F. E. C. (1971), "Non-Linear Growth and Limiting Amplitude of Acoustic Oscillations in Combustion Chambers", Combustion Science and Technology, **3**, 1-16.

Docquier, N., Candel, S. (2002), "Combustion control and sensors: a review", Prog. Energy Combust. Sci, **28**, 107-150.

Ganji, A. R., Sawyer, R.F. (1980), "An Experimental Study of the Flowfield of a Two-Dimensional Premixed Turbulent Flame", AIAA J., **18**(7), 817-824.

Ghoniem, A. F., Annaswamy, A., Park, S., Sobhani, Z. C. (2005), "Stability and emissions control using air injection and H2 addition in premixed combustion", Proceedings of the Combustion Institute, **30**, 1765-1773.

Kee, R.J., Rupley, F.M., Miller, J.A.(1989), "CHEMKIN-II: A Fortran chemical kinetics package for the analysis of gas-phase chemical kinetics", Sandia National Laboratories Report SAND89-8009.

Lee, J.G., Santavicca, D.A. (2003), "Experimental diagnostics for the study of combustion instabilities in lean premixed combustors", J. Propulsion and Power", **19**, 735-750.

Lee, S.Y., Seo, S., Broda, J.C., Pal, S., Santoro, R.J. (2000), "An experimental estimation of mean reaction rate and flame structure during combustion instability in a lean premixed gas turbine combustor", 28th Int. Symp. On Combustion", 775-782.

Lefebvre, A. H. (1995), ''The Role of Fuel Preparation in Low-Emission Combustion,'' ASME J. Eng. Gas Turbines Power, **117**, 617–654.

Pitz, R.W., Dailly, J.W. (1983), "Combustion in a turbulent mixing layer formed at a rearward facing step", AIAA J., **21**(11), 1565-1570.

Raffel, M., Willert, C., Kompenhans, J. (1998), Particle Image velocimetry. A Practical Guide, Springer, Berlin.

Rayleigh, J. W. S. (1945), The Theory of Sound, Vol. II, Dover Publications, New York, USA.